

Key design parameters and optimum method of medium- and high-velocity synchronous induction coilgun based on orthogonal experimental design

Kai-Pei Liu(刘开培), Xiao-Bo Niu(牛小波), Ya-Dong Zhang(张亚东), Zeng-Chao Ji(季曾超), Jian-Yuan Feng(冯建源), Wen-Qi Li(李文琦)

Citation: Chin. Phys. B . 2019, 28(2): 024102. **doi:** 10.1088/1674-1056/28/2/024102
Journal homepage: http://cpb.iphy.ac.cn; http://iopscience.iop.org/cpb

What follows is a list of articles you may be interested in

Real-space observation of individual skyrmions in helimagnetic nanostripes

Jin Chi-Ming, Du Hai-Feng
Chin. Phys. B . 2015, 24(12): 128501. **doi:** 10.1088/1674-1056/24/12/128501

Investigation of $L1_0$ FePt-based soft/hard composite bit-patterned media by micromagnetic simulation

Wang Ying, Wei Dan, Cao Jiang-Wei, Wei Fu-Lin
Chin. Phys. B . 2015, 24(6): 068504. **doi:** 10.1088/1674-1056/24/6/068504

Ablation and geometry change study of solid armature in a railgun

Zhang Ya-Dong, Ruan Jiang-Jun, Hu Yuan-Chao, Gong Ruo-Han, Wen Wu
Chin. Phys. B . 2013, 22(8): 084102. **doi:** 10.1088/1674-1056/22/8/084102

Micromagnetic simulation with three models of FeCo/$L1_0$ FePt exchange-coupled particles for bit-patterned media

Wang Ying, Wang Rui, Xie Hai-Long, Bai Jian-Min, Wei Fu-Lin
Chin. Phys. B . 2013, 22(6): 068506. **doi:** 10.1088/1674-1056/22/6/068506

Key design parameters and optimum method of medium- and high-velocity synchronous induction coilgun based on orthogonal experimental design*

Kai-Pei Liu(刘开培)[1], Xiao-Bo Niu(牛小波)[1,†], Ya-Dong Zhang(张亚东)[1], Zeng-Chao Ji(季曾超)[2], Jian-Yuan Feng(冯建源)[3], and Wen-Qi Li(李文琦)[3]

[1] *School of Electrical Engineering, Wuhan University, Wuhan* 430072, *China*
[2] *Electronic Information School, Wuhan University, Wuhan* 430072, *China*
[3] *College of Electrical and Electronic Engineering, Shandong University of Technology, Zibo* 255049, *China*

(Received 7 September 2018; revised manuscript received 24 November 2018; published online 10 January 2019)

The energy conversion efficiency of a multistage synchronous induction coilgun (MSSICG) has become one of the key factors that restricts its industrialization. To improve the launch efficiency of medium- and high-velocity MSSICG, we propose an optimization design scheme combining orthogonal experimental design (OED) and self-consistent design method in this paper. The OED is introduced to reduce the number of iterations and improve the identification accuracy and efficiency. A self-consistent design model is established to overcome a defect that the parameters that need to be optimized will multiply as the number of coil stages increases. The influence of six factors (radial thickness of armature, axial length of armature, axial length of coil, capacitance, wire diameter, and slip speed) on the launch efficiency are then evaluated by range analysis. This work presents a valuable reference for optimizing medium- and high-velocity MSSICG.

Keywords: multistage synchronous induction coilgun (MSSICG), self-consistent design, orthogonal experimental design (OED), range analysis

PACS: 41.75.Lx, 85.70.Ay, 85.70.Rp **DOI:** 10.1088/1674-1056/28/2/024102

1. Introduction

An electric energy-driven electromagnetic launcher (EML) can transform electromagnetic (EM) energy into mechanical kinetic energy. EML has been considered as another revolution of launching theory, following the development of mechanical- and chemical-energy launching weapons. It has the advantages of low launching cost, simplified logistics, flexible velocity regulation, high precision, *etc*.[1,2] Therefore, EML technology has promising application prospects in both civilian and military fields. Recent typical applications of EML in passenger transport can be seen on the No. 4 and No. 5 linear metro in Guangzhou, China.[3] The Applied Superconductivity Laboratory (ASCLab) of Southwest Jiaotong University is studying an evacuated tube high-speed maglev to enhance the train speed to 2900 km/h.[4] It is shown in Ref. [5] that an electromagnetic launcher can be used to assist civil aircraft take-off. The University of Texas has demonstrated the use of a 64-state coilgun to decelerate a metastable neon atom beam from 447 m/s to 55.8 m/s.[6] However, there is no doubt that the military application is the main intention of the proposed concept of EML, which is also the most effective reflection of its value and prospect. The U.S. military hopes to apply EML to future combat systems with the development of EM mortar.[7] Active EM armor based on EML can significantly enhance the defense capabilities of modern weapon systems.[8] Sandia National Laboratories and Lockheed Martin MS2 have jointly developed a new electromagnetic missile launcher, which can not only eliminate the danger posed by gunpowder but can also simplify the logistics and reduce the cost of operation and maintenance.[9] In 2004, the U.S. replaced its traditional steam catapult with an EM aircraft launch catapult on its carriers.[10] In terms of strategic defense, space-based EML can be used to intercept mid-range, submarine-launched and intercontinental ballistic missiles. It can even be used to attack enemy satellites and space stations. Its implementation will be simpler than high-energy laser weapons.[11,12]

A synchronous induction coilgun (SICG) is one of the most promising research aspects in EML research because of its outstanding non-contact linear propulsion performance.[13,14] The basic mechanism of the SICG is to accelerate the projectile by the Lorenz force generated by the interaction between the traveling magnetic field and the induced current. Although it seems to be very simple, the launching process is a multi-field coupled process that involves many parameters, including electrical parameters and structural parameters. Therefore, it is difficult to achieve high-velocity and high-energy conversion efficiency by global optimization. To improve the performance of SICG, the genetic algorithm,[15] second-generation non-dominated sorting

*Project supported by the National Natural Science Foundation of China (Grant No. 5140130).
†Corresponding author. E-mail: 1215409612@qq.com
© 2019 Chinese Physical Society and IOP Publishing Ltd

genetic algorithm,[16] and ant colony algorithm[17] have been used to optimize the parameters of the launcher.

The introduction of heuristic intelligent algorithms will improve the launch performance to some extent. However, the parameters to be optimized will multiply as the number of coil stages increase, followed by extensive and time-consuming calculation work. In addition, these intelligent algorithms cannot reflect the effect of each parameter on the performance of the system. In single-factor analysis,[18–21] the coupling and constraint relationships among parameters are ignored, although it has higher computational efficiency and reflects the specific parameter's influence on the launcher performance. Therefore, their ability to guide the design of an MSSICG is limited. Some researchers have used the orthogonal experimental design (OED) to seek the optimal parameter combination and they have tried to analyze the influences of various factors on the performance of the whole system, but it is indicated that these researches are only limited to the case of one or more coil-driven low-speed launcher.[22–25]

In this work, we propose a combination of OED and self-consistent control model, which is different from the low-speed SICG that was used in previous work, to optimize the performance of medium- and high-velocity MSSICG. First, the self-consistent design model based on the current filament method (CFM) is established and its validity and flexibility are verified by the finite element method (FEM). Our model combines the systematic differential equations and governing equations, and then the turns and the triggering sequence of each driving coil can be calculated. Therefore, the main advantage of introducing self-consistent control model is that the optimization parameters will not multiply with the increase of the coil stage. Second, the energy conversion efficiency of the MSSICG with the combination of different parameters is calculated based on OED. Finally, a range analysis is carried out for the test data at the end of the test. This enables us to distinguish between the major factor and minor factor, and even indicate the adjustment direction of each factor when designing the medium- and high-velocity SICG, which provides a valuable reference to further improve the launch performance of the MSSICG.

2. Self-consistent model of MSSICG

As shown in Fig. 1, MSSICG consists of discrete solenoidal driving coils, power supply, armature, freewheeling diode, trigger switch, *etc*.[26] A magnetic traveling wave in the barrel is produced by discharging a series of capacitors sequentially, which will induce opposite currents in the armature without direct electrical contact between the barrel and projectile. According to Lenz's law, the interaction between the induced current and the radial magnetic wave generates electromagnetic force that accelerates the armature.[24] The load-side crowbar diode not only prevents the capacitor from damage due to voltage reversal caused by the inductive load during the pulsed power supply period but also blocks the induced current caused by the previous stator coil.[27]

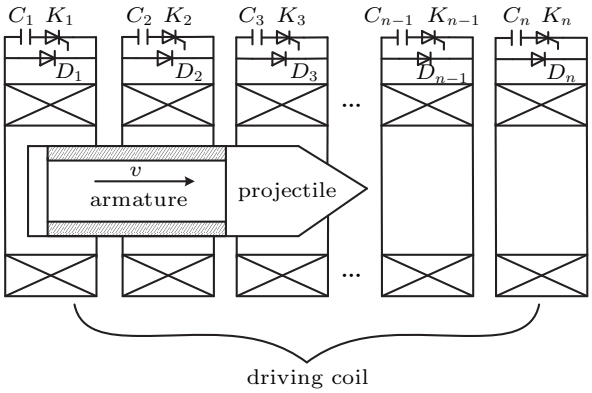


Fig. 1. Schematic diagram of the MSSCIG.

2.1. Systematic differential equation

The launch process of the MSSICG involves complex multi-physics field dynamic coupling problem.[25] Therefore, it is necessary to establish a simulation model considering both convenience and accuracy. The current filament method described by Tao *et al.* in Ref. [15] has been widely accepted thanks to its distinctive features, such as simple principle, clear concept and easy programming. In this method, the driving coil and the armature can be divided into sub hollow column hoops in which the current distribution may be relatively uniform in the radial direction in the case without considering the skin-effect. Each hoop can be regarded as a separate element because the current flowing in each hoop is different. The equivalent network of the MSSICG based on the current filament method is shown in Fig. 2.[28]

The electrical and mechanical equations used to describe the behaviors of the system can be formulated as ordinary differential equations with nonlinear variable coefficients,[27] which can be solved by fourth-order Runge–Kutta method,

$$\{[L]+[M]\}\frac{\mathrm{d}[I]}{\mathrm{d}t}=[V_c]-[R]\cdot[I]-v\left[\frac{\mathrm{d}M}{\mathrm{d}x}\right]\cdot[I], \quad (1)$$

$$[C]\frac{\mathrm{d}[V_c]}{\mathrm{d}t}=-[I_d], \quad (2)$$

$$m\frac{\mathrm{d}v}{\mathrm{d}t}=\sum_{p=1}^{m}\sum_{d=1}^{n}I_pI_d\frac{\mathrm{d}M_{pd}}{\mathrm{d}x}, \quad (3)$$

$$\frac{\mathrm{d}x}{\mathrm{d}t}=v, \quad (4)$$

in the above expressions, $[I]$ is the column vector composed of the coil current and the current filament current; $[R]$ is the diagonal matrix formed by the current filament resistance and the coil resistance; $[L]$ is the diagonal matrix formed by the current filament inductance and the coil inductance; each element of $[M]$ represents a mutual inductance between any two

individual coils; $[C]$ and $[V_c]$ are the capacitance of the capacitor and its terminal voltage, respectively; and m, v_p, and z are the mass, the velocity, and the displacement of the armature, respectively.

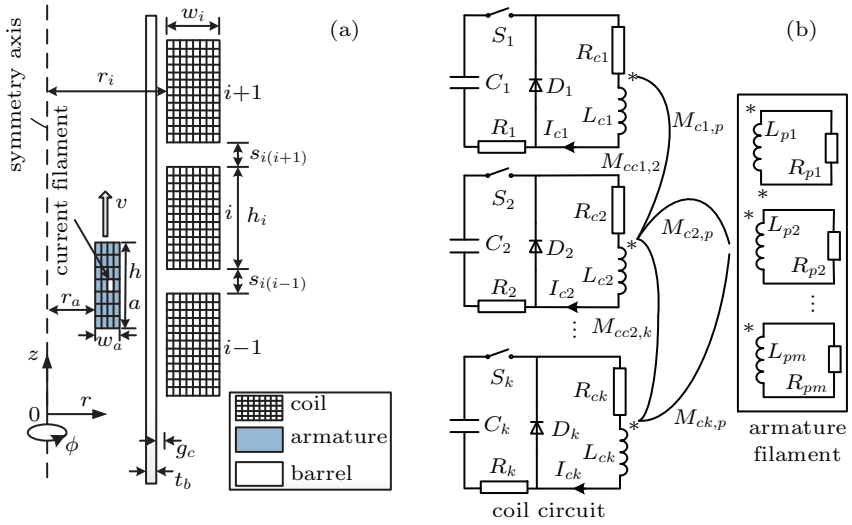


Fig. 2. Schematic of CFM Showing (a) CFM of coilgun and (b) Equivalent circuit.

2.2. System control equation

For the low-speed coilgun driven by a few driving coils, the number of turns and the corresponding trigger time are usually obtained by step-by-step debugging. However, with the increase of the number of the coil stages and the armature speed, the trigger timing control and the power regulation become more complicated, while the control effect of traditional trigger strategy is unsatisfactory. Therefore, the solution model of the medium- and high-velocity MSSICG studied in this paper is replaced by self-consistent calculation method.[29]

The feeding of the driving coil must be kept in synchronicity with the moving position of the armature, which is crucial for whether the launcher can accelerate a projectile to a high speed.[30] It is expectable that the pulse current just reaches its peak value when the distance from the tail of the armature to the center of the driving coil is a specified slip distance.[31] This means that at the triggering moment of the coil, the distance between the tail of the armature and the center of the coil is the sum of the slip distance and the rise distance. The intuitive representation of this conclusion is shown in Fig. 3.[32]

$$\begin{cases} Z_{ck} - Z_a \le Z_{\text{slip}} + \lambda_k, \\ Z_{\text{slip}} = v_{\text{slip}} t, \end{cases} \tag{5}$$

where Z_{ck} is the position of the k-th coil center, Z_a is the position of the armature tail, v_{slip} and Z_{slip} are the slip speed and slip distance, respectively, λ_k is the distance that the armature moves during the pulsed current rise time of k-th driving coil; *i.e.*, the rise distance.

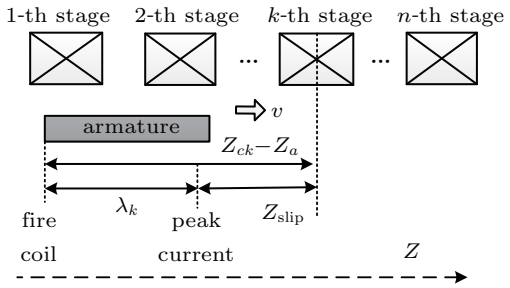


Fig. 3. Location on armature of coil firing.

The driving coil branch can be regarded as the resistor–inductor–capacitor (R–L–C) circuit and the frequency of discharge current can be defined as follows:

$$f = (2\pi N\sqrt{L_1 C})^{-1}, \tag{6}$$

where N is the number of turns, L_1 is the equivalent single-turn inductance, and C is the capacitance of the discharge circuit.

To keep the acceleration reasonably smooth, the distance that the armature moves during the current rise time should be no less than twice the center distance of the coil, to ensure that at least two coils act simultaneously in the acceleration process of the armature. The rise length corresponding to k-th stage driving coil can be defined as follows:[31]

$$\lambda_k = sl, \tag{7}$$

where l represents the center distance of two adjacent coils, the value of coefficient s should be set to make sure that not only the number of stage but also the difference in turn between two adjacent coils is as small as possible.

Assume that the armature velocity is constant during the rise time of the discharge current, the distance that the armature moves during the rise time of the k-th coil current is

$$\lambda_k = v\tau_k = v\frac{\pi N\sqrt{\beta L_1 C}}{2}, \tag{8}$$

where the factor β reflects the effect of armature motion on the equivalent inductance of the driving coil. In this paper, we set it to 0.5.

The number of turns of k-th driving coil derived from the above Eq. (8) is shown in the following equation:

$$N_k = 2\lambda_k(\pi v\sqrt{\beta L_1 C})^{-1}. \tag{9}$$

The acceleration of the armature from rest will result in a large number of coil turns calculated according to Eq. (9). The fundamental cause is that during this time, the magnetic traveling wave has not been completely established. In other words, the obvious slip speed between the traveling wave and the armature has not been established. However, the armature is usually not set to be a non-zero initial speed in engineering practice. So, we divide the entire design process into two phases, as shown in Fig. 4. The first N_1- stage driving coils were debugged step-by-step in the first phase, and then other multistage driving coils were calculated by the self-consistent method in the second phase.

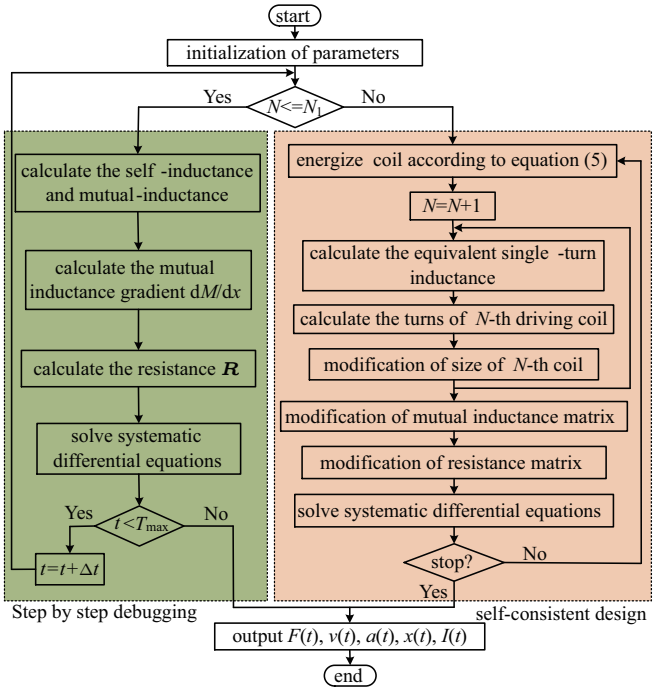


Fig. 4. General design process of MSSICG.

It should be pointed out that in WARP-10[33] and SLINGSHOT,[34] the coils with different turns were approximately considered to have the same radial thickness, and then the equivalent single-turn inductance of all coils was the same. However, the error of this approximate calculation increases as the difference in the number of radial layers increases. Therefore, it is considered that only the equivalent single-turn inductance values of two adjacent coils are equal in the self-consistent design strategy proposed in this paper, so that the turns of the next-stage coil can be calculated according to the size of the upper-stage coil, and then the size of the next-stage coil is adjusted. The whole calculation flow chart is shown in Fig. 4. When the difference in the radial layers of the coils cannot be neglected, the radial thickness values of two adjacent coils are approximately equal, which to a certain extent reduces the calculation error.

2.3. Verification

Usually, prototype tests or finite element models are used to validate the circuit model of MSSICG. However, the MSSICG used in medium-high velocity launching has higher requirements for the performance of hardware, so the prototype test is expensive and time-consuming. In terms of FEM-based transient field-circuit coupling model, not only the spatiotemporal distribution of each field can be obtained but also the calculation accuracy can be higher than that when using the lumped-circuit model.[35] Therefore, the validity and the flexibility of the design model of MSSICG mentioned above were verified by the transient field-circuit coupling model.

The parameters of the 45-stage coilgun used for verification are listed in Table 1. As mentioned above, the whole design flow chart of the MSSICG is divided into the step-by-step debugging part of the first N_1 stages and the self-consistent calculation part of the other coils. In Ref. [16], we have verified the effectiveness of the program based on the step-by-step debugging method. To verify the self-consistent design program, we set an initial speed to be 200 m/s for the armature to avoid the tedious debugging of the previous stages.

Table 1. Simulation parameters of 45-stage coilgun.

Component	Parameter	Value
Driving coil	inner radius	2.65 cm
	axial length	3.0 cm
	number of stages	45
	space	1.0 cm
	diameter of wire	1.5 mm
	insulation thickness of wire	1.5 mm
Armature	outer radius	2.2 cm
	axial length	10 cm
	radial thickness	4.0 mm
	mass	135 g
	material	aluminum
External circuit	voltage	3.7 kV
	capacitance	1.5 mF
	resistance	10 mΩ
	total energy storage	455 kJ

The topology of the excitation circuit in ansoft Maxwell circuit editor is shown in Fig. 5(a). Limited by space, only part of the simulation model of the 45-stage coil is intercepted as shown in Fig. 5(b).

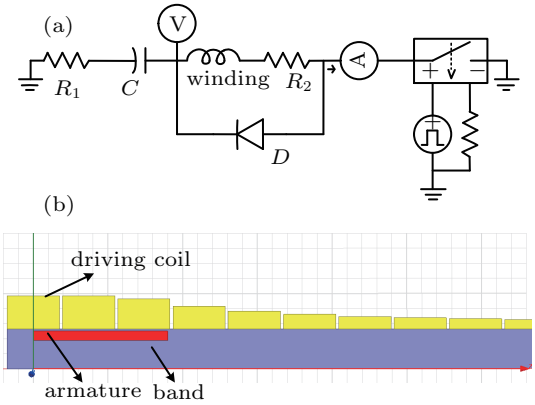


Fig. 5. Transient field-circuit coupling model of 45-stage coilgun, showing (a) topological diagram of the excitation circuit, and (b) simulation model of 45-stage coilgun.

A comparison in the velocity and displacement characteristics of the armature is shown in Fig. 6. It can be observed in the figure that the muzzle velocities obtained by the self-consistent design scheme and the finite-element verification model are 867 m/s and 874 m/s respectively, and the discrepancy between them is 0.8%. Good alignment of the displacement curve can also be obtained. These results are sufficient to verify the accuracy of the self-consistent design scheme proposed in this paper.

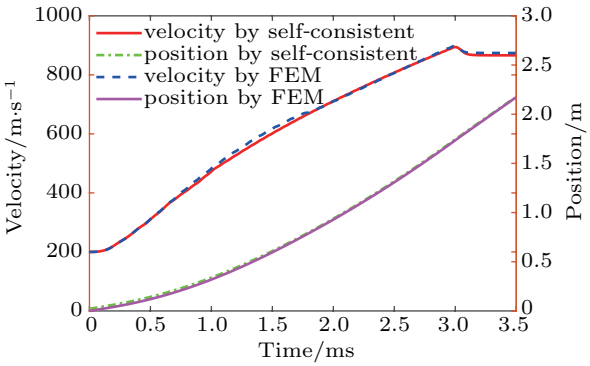


Fig. 6. Comparison of time-dependent velocity and displacement curves of the armature, obtained by self-consistent design scheme and finite-element model.

3. Orthogonal design of experiments

The OED is usually used for characterizing and optimizing system performances in many research fields involving multivariate and multilevel factors. In orthogonal tests, a representative subset with the characteristics of uniformly dispersing across the data set and neat comparison was selected from the full factorial combinations. This statistical analysis technique can evaluate the influence of relevant factors on the experimental index and rank them by their effects. This has been demonstrated to be an efficient, fast, and economical experimental design method.[36]

The key of OED is to utilize an orthogonal table to arrange the experiment scientifically and evaluate multiple factors. The general expression of the orthogonal table is $L_n(t^q)$, where L is the symbol of orthogonal design, n denotes the number of experiments (rows), t and q represent the number of levels and the number of factors (columns), respectively.

Generally, two analytical methods are used to analyze orthogonal test results: range analysis (also called intuitive analysis) and variance analysis (also known as statistical analysis). Compared with the latter, the former avoids conducting a series of complicated processing calculations without reducing the statistical significance, which makes it more practicable.[37] The range refers to the difference between the maximum and minimum of the average of the experimental indexes corresponding to each level in each column. The mathematical expression is as follows:[24]

$$R_j = \max\left\{\left(\sum_{i=1}^{n} J_i\right)\Big/ n\right\} - \min\left\{\left(\sum_{i=1}^{n} J_i\right)\Big/ n\right\}, \quad (10)$$

where j is the column number, i is the level number in j-th column, n is the number of times the i-th level occurs, and J_i is the test index value corresponding to the i-th level.

According to the range analysis in OED, the following results can be obtained:

(i) The influence degree of each factor on the test index;

(ii) The tendency of the test index value to change with each factor;

(iii) The most appropriate combination of levels that can make the test index reflect the highest significance.

Taking the 45-stage SICG system shown in Fig. 5(b) as an example, we use the OED to study the parameter optimization design of the medium- and high-velocity MSSICG. When considering the interaction between parameters, the most important parameters of the launch efficiency can be obtained. To arrange the simulation experiments scientifically for the SICG, the following should be done: clarify the experimental objectives, choose the controllable design variables and levels, and construct an appropriate orthogonal table.

3.1. Factors and levels

The pulsed power supply, armature, driving coils and corresponding trigger timing are four components of the MSSICG. The space between the adjacent coils and the gap between coil and armature can be fixed values which are limited by the material and technological level. The parameters of the hollow aluminum armature and the total pulse energy storage are consistent with those in Table 1. The turns of driving coils and their corresponding trigger time are calculated by the self-consistent program. Therefore, we select six parameters as the factors including the axial length of the armature, the thickness of the armature, the axial length of the driving

coil, the diameter of the wire, the capacitance value and the slip speed. Although the muzzle velocity can be increased by enlarging the energy storage of the capacitor bank, in practical engineering, especially for a high velocity launcher with a large number of stages, the cost in pulsed power supply is too high. Therefore, improving energy conversion efficiency is of substantial significance to reduce cost and equipment volume. The energy conversion efficiency selected as the test target function can be defined as follows:

$$\begin{aligned}\eta &= (1/2)\left(mv^2 - mv_0^2\right) \Big/ \left((1/2)\sum_{i=1}^{n} C_i U_{0i}^2\right) \\ &= f\left(w_a, q, l_c, D, C, v_{\text{slip}}\right), \end{aligned} \tag{11}$$

where w_a is the thickness of the armature, q represents the ratio of armature length to coil length, l_c is the axial length of the driving coil, D is the diameter of the wire, C is the capacitance value, v_{slip} is the slip speed, m and v are the mass and initial velocity of the armature. The total energy storage of the pulsed power supply is constant, so the charging voltage of the capacitor bank with a specified capacitance can be expressed as follows:

$$U_{0i} = \sqrt{2W_c/(nC_i)}, \tag{12}$$

where W_c is the total energy storage of all capacitor banks, and n is the number of coil stages.

After the factors are selected, the expected number of levels can be determined to introduce an appropriate orthogonal table. The influence factors and levels selected in this study are summarized in Table 2.

Table 2. Factors and levels.

Levels	Factors					
	w_a/cm	q	l_c/cm	C/mF	D/mm	v_{slip}(m/s)
1	3.0	1.0	2.5	0.5	1.5	5.0
2	4.0	2.0	3.0	1.0	2.0	9.0
3	5.0	3.0	3.5	1.5	2.5	13.0
4	6.0	4.0	4.0	2.0	3.0	17.0
5	7.0	5.0	4.5	2.5	3.5	21.0

3.2. Orthogonal table

The orthogonal design table $L_{25}(5^6)$ as shown in Table 3 is adopted because the selected array ($L_{25}(5^6)$) matches well with the selected number of factors and levels (only part of arrangements are shown due to limited space). There are $56 = 15625$ simulation cases to be built if full-scale experiment is applied. Matlab-based program takes about 8 minutes to run a test (CPU: Intel(R) Xeon (R) E5-2620 v4 @2.1 GHz 2.1 GHz; RAM: 64 GB), so full-scale experiment takes nearly 87 days, while FEM-based test takes longer. Even in the design phase rather than on-site operation, the time consumption is unacceptable. This paper focuses on the effect of the parameters on the launch performance. Therefore, the interaction between the parameters is not considered.

Table 3. Orthogonal table.

Column	1	2	3	4	5	6	Result
Test \ Factor	w_a	q	l_c	C	D	v_{slip}	
1	3.0	1.0	2.5	0.5	1.5	5.0	5.05%
2	3.0	2.0	3.0	1.0	2.0	9.0	5.88%
3	3.0	3.0	3.5	1.5	2.5	13.0	7.72%
4	3.0	4.0	4.0	2.0	3.0	17.0	6.88%
5	3.0	5.0	4.5	2.5	3.5	21.0	6.76%
6	4.0	1.0	3.0	1.5	3.0	21.0	2.45%
7	4.0	2.0	3.5	2.0	3.5	5.0	4.89%
8	4.0	3.0	4.0	2.5	1.5	9.0	3.30%
9	4.0	4.0	4.5	0.5	2.0	13.0	6.92%
10	4.0	5.0	2.5	1.0	2.5	17.0	12.2%
...	...	...	...	...	...	...	...
25	7.0	5.0	4.0	1.5	2.0	5.0	5.35%
k_1	6.46	3.0	8.09	8.89	5.54	5.49	
k_2	5.95	5.13	7.45	7.18	5.34	6.35	
k_3	5.97	7.71	7.12	5.26	6.86	6.33	
k_4	5.87	7.84	4.77	5.39	6.75	7.39	
k_5	7.76	7.74	4.59	5.0	7.53	6.45	
R	1.89	4.84	3.50	3.89	2.19	1.90	

3.3. Results and discussion

The average value of each level in each column and the range of each factor were calculated based on Eq. (10). The results of the range analysis are shown in Fig. 7. Generally, when the range is larger, the corresponding parameter sensitivity is higher.[38] In other words, the effect of the parameter on the launching efficiency is more significant when its range is larger. From Fig. 7, it can be seen that for the energy conversion efficiency of the medium-high velocity SICG, the importance of the various factors is ranked as: axial length of the armature > capacitance value > axial length of the coil > wire diameter > slip speed > thickness of the armature.

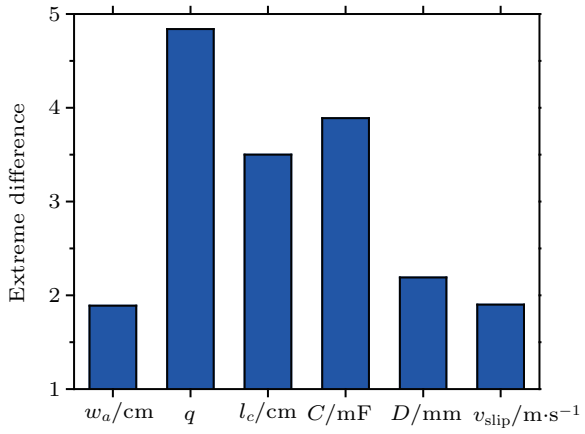


Fig. 7. Histogram of range analysis of each factor.

The intuitive analysis effect curve of each factor on the performance index of the medium-high velocity SICG can be

obtained according to the range analysis as shown in Fig. 8. We can draw some useful conclusions, as follows.

i) In terms of medium-high velocity SCIG, the optimal length of the armature should be 3–4 times the coil length, which is different from 2–2.5 times in low-speed case.[20]

ii) Generally speaking, the larger the wire diameter, the higher the launch efficiency is. This conclusion is consistent with that obtained in Ref. [24], which used the OED to optimize the low-speed launch. The efficiency is lower when the capacitance is higher (which means a lower voltage).

iii) The variation of efficiency with the slip speed is approximately parabolic. A small slip speed indicates that the magnetic traveling wave has a small velocity in advance of the armature, which results in the driving coil not being fed in time. Also, the coupling between the coil and armature will be weakened. However, excessive slip speed means that the coil is fed prematurely, which leads to peak current position exceeding the armature front, resulting in a reverse thrust that deteriorates the launch performance.

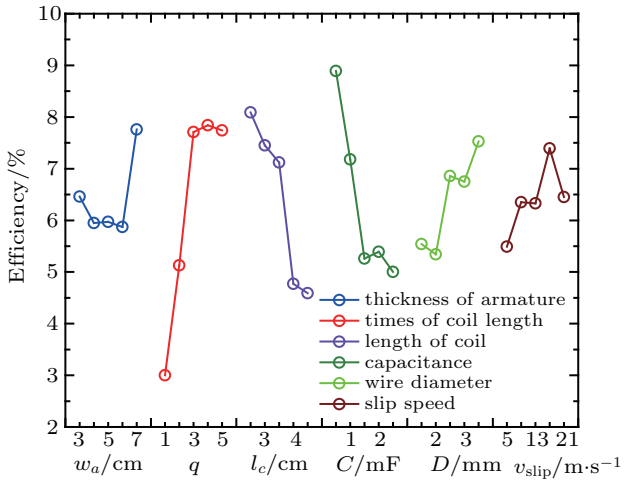


Fig. 8. Intuitionistic effect curve of influence factors.

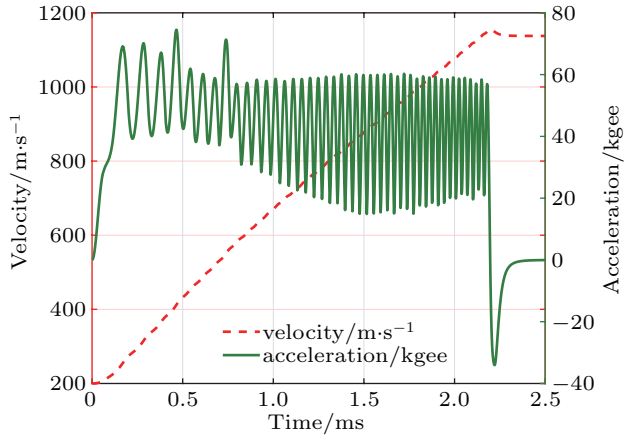


Fig. 9. Armature acceleration and velocity characteristic curves.

The optimal values of the parameters to improve the efficiency are given as follows: $w_a = 7$ mm, $l_c = 2.5$ cm, $q = 4$, $D = 3.5$ mm, $C = 0.5$ mF, and slip $= 17$ m/s. This combination is not included in Table 3 because the combination of controllable parameters at the set level cannot cover all possible cases. Therefore, we perform the self-consistent design program with the optimal combination above, and the obtained acceleration and velocity characteristic curve are shown in Fig. 9. A comparison of parameters and performance index before and after optimization is shown in Table 4.

Table 4. Comparison of parameters and performance indicator.

Item	w_a/mm	q	l_c/cm	D/mm	C/mF	v_{Slip}/(m/s)	η/%
Before	4.0	3.3	3.0	1.5	1.5	13	11.1
After	7.0	4.0	2.5	3.5	0.5	17	18.6

4. Conclusions and perspectives

In this paper, the improved self-consistent design scheme of medium-high velocity MSSICG is illustrated. Our method can solve the turn number and trigger timing of the driving coil. Consequently, the parameters to be optimized will not multiply as the number of coil stage increases. The accuracy of Matlab-based program is verified by the transient field-circuit coupling model based on FEM. Then, the orthogonal experimental design is introduced to analyze the parameter optimization of a 45-stage coilgun. With the total capacitance storage fixed at a constant, the axial length and the thickness of the armature, the axial length of the coil, the wire diameter, the capacitance, and the slip speed are regarded as variables. The energy conversion efficiency is selected as a target function. The range analysis is employed to evaluate the influences of various factors on launch efficiency. The major conclusions are summarized as follows:

(I) Among all the factors affecting the launch efficiency, the axial length of the armature is the most important, and the next sequentially are the capacitance value, axial length of the driving coil, wire diameter, slip speed, and finally thickness of the armature.

(II) The best length of the armature should be 3–4 times the coil length.

(III) When the total capacitive energy storage is constant, the energy conversion efficiency is higher when the capacitance is lower (*i.e.*, the higher the voltage).

(IV) The smaller coil length is more conducive to the coupling between the armature and the coil, thereby enhancing the launch performance.

(V) The variation of energy conversion efficiency with slip speed is approximately parabolic.

Acknowledgment

We thank Tingting Zheng for taking part in the revision of our English grammar.

References

[1] Ma W M and Lu J Y 2017 *IEEE Trans. Plasma Sci.* **45** 1071
[2] Shurdal B D and Gaigler R L 2009 *IEEE Trans. Magn.* **45** 458
[3] Lu J Y and Ma W M 2011 *IEEE Trans. Plasma Sci.* **39** 116
[4] Deng Z G, Zhang W H, Zheng J, *et al.* 2016 *IEEE Trans. Appl. Supercond.* **26** 3602408
[5] Bertola L, Cox T, Wheeler P, Garvey S and Morvan H 2016 *IEEE Trans. Appl. Supercond.* **26** 3602911
[6] Narevicius E, Libson A, Parthey C G, Chavez I, Narevicius J, Even U and Raizen M G 2008 *Phys. Rev. Lett.* **100** 093003.1
[7] Turman B N, Kaye R J and Crawford M 2006 25*th Army Sci Conf.* 1
[8] Sterzelmeier K, Brommer V and Sinniger L 2001 *IEEE Trans. Magn.* **37** 238
[9] Aubuchont M S, Lockner T R and Turman B N 2005 *IEEE Int. Pulsed Power Conf.* 75
[10] Lu J Y, Ma W M, Zhang X, Long X L and Tan S 2016 *IEEE Trans. Plasma Sci.* **44** 2211
[11] Fair H D 2015 *IEEE Trans. Plasma Sci.* **43** 1112
[12] Schoeder J M, Gully J H and Driga M D 1989 *IEEE Trans. Magn.* **25** 504
[13] Kolkert W J and Jamet F 1999 *IEEE Trans. Magn.* **35** 25
[14] Zhang Y D, Ruan J J, Hu Y C, Gong R H and Wen W 2013 *Chin. Phys.* **22** 084102
[15] Tao X, Wang S H, Huangfu Y P, Wang S and Wang Y Q 2015 *IEEE Trans. Plasma Sci.* **43** 1028
[16] Niu X B, Liu K P, Zhang Y D, Xiao G and Gong Y J 2017 *IEEE Trans. Plasma Sci.* **45** 1622
[17] Liu W B, Cao Y J, Zhang Y, Wang J and Yang D W 2011 *IEEE Trans. Plasma Sci.* **39** 100
[18] Cao Y J, Liu W B, Li R F, Zhang Y and Zou B G 2009 *IEEE Trans. Magn.* **45** 518
[19] Xiang H J, Yuan J S, Gao X B and Li Z Y 2012 *6th Int. Conf. on Electromagn. Field Problems and Appl.*
[20] Zhang Y D, Xiao G, Gong Y J, Niu X B and Liu K P 2017 *IEEE Trans. Plasma Sci.* **45** 1574
[21] Zhu Y W, Yan Z M, Dong L and Wang Y 2009 *High Voltage Engineering* **35** 3054 (in Chinese)
[22] Xiang H J, Lei B, Li Z Y and Zhao K Y 2015 *IEEE Trans. Plasma Sci.* **43** 1198
[23] Zhang Y J, Liu K P, Liao J P, Zhang Y D, Wu C L and Hu Y C 2012 *16th Int. Symp. Electromagn. Launch Technol.*
[24] Zhang Y D, Ruan J J, Niu X B, Tan T Y and Wen W 2015 *IEEE Trans. Dielect. Elect. Insul.* **22** 2073
[25] Le D V, Go B S, Song M G, Park M and Yu I K 2018 *IEEE Trans. Plasma Sci.* **46** 3612
[26] Zhang T, Guo W, Su Z Z, Cao B, Ren R, Li M T, Ge X and Li J X 2015 *IEEE Trans. Plasma Sci.* **43** 1203
[27] He J L, Levi E, Zabar Z and Birenbaum L 1989 *IEEE Trans. Plasma Sci.* **17** 429
[28] Liu S B, Ruan J J, Peng Y, Zhang Y J and Zhang Y D 2011 *IEEE Trans. Plasma Sci.* **39** 382
[29] Niu X B, Liu K P, Zhang Y D, Xiao Z R, Xiao G and Gong Y J 2018 *Energy* **144** 1
[30] Wang M, Cao Y J, Wang C X, Wang H J and Chen J L 2016 *IEEE Trans. Plasma Sci.* **44** 885
[31] Marder B 1993 *IEEE Trans. Magn.* **29** 701
[32] Shokair I R, Cowan M, Kaye R J and Marder B M 1995 *IEEE Trans. Magn.* **31** 510
[33] Winder M M 1991 *IEEE Trans. Magn.* **27** 634
[34] Kaye R J 2005 *IEEE Trans. Magn.* **41** 194
[35] Liu S B, Ruan J J, Du Z Y, and Huang D C 2010 *Transactions of China Electrotechnical Society* **25** 1 (in Chinese)
[36] Ji L J, Si Y F, Liu H F, Song X L, Zhu W and Zhu A P 2014 *Microporous Mesoporous Mater.* **184** 122
[37] Tu Y P, Luo M X, Ying G F and Ding L J 2012 *Proc. CSEE* **32** 139 (in Chinese)
[38] Li Y Y and Hu C R 2005 *Experiment design and data processing* (Beijing: Chem. Ind. Press) p. 62 (in Chinese)